Electronic Supplementary Material

For

Manifestation of Site Energy Landscapes for Ion Transport in Borate Glasses

Victor H. Gunawan, Martin Schäfer, Karl-Michael Weitzel*

Philipps-Universität Marburg, Chemistry Department; Hans-Meerwein Str. 4,
35043 Marburg, Germany

Corresponding author: weitzel@chemie.uni-marburg.de

Table of Contents

1. Materials

1.1 Sample preparation

Lithium borate glass with a composition of 30% Li_2O and 70% B_2O_3 ($Li_3B_7O_{12}$) is prepared by means of the melt-quenching method.[1,2] Lithium carbonate is first dried for 12 h at 110°C and then mixed with boric acid. The mixture is ground thoroughly in an agate mortar and subsequently poured into a platinum crucible. The mixture is then slowly heated to 1100°C to slowly release water vapor and carbon dioxide from the reagents. In order to obtain a homogeneous melt, the heating process continues for 2 h at the same temperature. Afterwards, the melt is poured into a mold at a temperature of 450°C. The formed glass is relaxed at the same temperature for 15 h and then cooled slowly to 80°C to prevent breaking the glass. The product is removed from the mold and is cut into discs with a cutting machine (Mecatome T180, PRESI). The sample is then polished

at both sides with a polishing machine (LaboPol-5, Struers) as well as polishing cloths (PT Plan S, CLOEREN TECHNOLOGY GmbH) and paste (6-KD-C3 and 3-KD-C3, Kemet). Samples with a thickness between 1.9 - 2.7 mm were obtained at the end of this process. For improving the electrical contact between the sample and the copper electrode, the back side of the sample is sputter coated (EM ACE600, Leica) with a 100 nm thick platinum layer and covered with silver paste (Heat-Away 641-EV, Kager GmbH).

2. Methods

2.1 Charge-Attachment Induced Transport (CAIT)

The back side of the sample is attached to a single grounded electrode, while an ion beam (K^+, Rb^+ or Cs^+) is directed onto the front side of the sample. Once the ions arrive at the sample front surface, they softly attach and charge the surface. A well-defined (positive) electric potential and surface ion density establish, leading to a potential and concentration gradient that drive the motion of the positive charge carriers towards the grounded back-side electrode. Negative charge carriers are not mobile in the samples. Positive charge carriers arriving at the back side are neutralized and ultimately form a metal layer at the interface between the sample and the back-side electrode. After a short time, a stationary state forms where for every charge carrier neutralized at the back side, a charge carrier from the beam is attached to the front side of the sample. In this situation, the electric potential, the recorded current and the charge carrier concentration attached to the surface of the sample become time-independent. Ultimately, there is a quasi-stationary cloud of charge carriers present in front of the sample surface which from the viewpoint of transport theory represents an infinite source and from the viewpoint of electrochemistry represents a virtual electrode.

In the course of this macroscopic, time-dependent transport experiment, ions from the external ion beam enter the sample surface, occupying sites that have been abandoned by the Lithium ions moving towards the sample back side in a push-pull process. As a consequence, a depletion / replacement zone evolves, where foreign ions (i.e. K^+, Rb^+ or Cs^+ ions) have replaced native Li^+ ions.

2.2 Time-of-Flight Secondary Ion Mass Spectrometry (ToF-SIMS)

The depletion / replacement zones evolving during the CAIT experiment are ex-situ quantified by means of chemical microscopy, where concentration – depth profiles were measured by Time-of-Flight Secondary Ion Mass Spectrometry (ToF-SIMS). ToF-SIMS measures the chemical composition with very high mass resolution (m/Delta_m = 15000) and single-particle counting characteristics. The measurement process involves repetitive analysis and sputtering cycles providing a depth resolution in the transport direction of better than 2nm.

During the analysis cycle, a Bi^+ ion beam with a current of 1 pA is used to analyze the sample on an area of 100 x 100 µm in 128 by 128 spots. The secondary ions are then abstracted and analyzed with a time-of-flight mass spectrometer. The mass spectrum yields the composition of the material. The results from the 128 by 128 spots are summed up to obtain the average composition of the entire layer. Subsequently, the sample surface is removed employing an O_2^+ beam with a current of around 80 nA onto a 300 x 300 µm area, making the layer beneath accessible for the Bi^+ ion beam. The bigger area for the sputtering process is chosen to prevent artificial edge

effects from the formed crater. By applying both beams alternatingly, a concentration-dependent intensity of the studied fragments is measured as a function of sputtering time. An electron flood gun is also applied during the measurement for compensating the charge build-up during the sputtering process.

5

2.3 Transfer of raw-data into concentration profiles

The result of the ToF-SIMS analysis yields data in the format "Poisson-corrected counts as function of sputter seconds". In order to transfer the data into quantitatively evaluable data, a normalization procedure is applied.

10

In a first step of this procedure, the traces of all stable isotopes of the desired elements are summed up. This applies for Li (^{6}Li+^{7}Li), K (^{39}K+^{41}K) and Rb (^{85}Rb+^{87}Rb). ^{133}Cs is the only stable Cs isotope. These raw data are shown in Fig. S1.
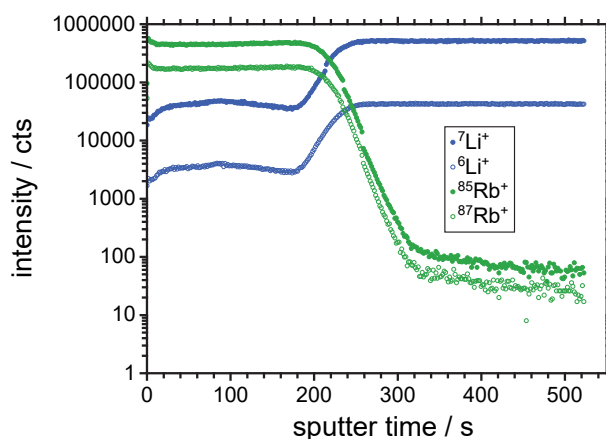
Fig. S1.

Raw data of the Rb-CAIT experiment. *The graph shows the raw data of the Rb-CAIT experiment. In blue the two Li isotopes and in green the two Rb isotopes are shown. Rb has replaced a significant amount of the native Li in the first 200 nm below the sample surface.*

20

The depth axis can be calibrated by measuring the crater depth of the ToF-SIMS crater by means of a tactile profilometer (Bruker DektakXT). The total sputter time corresponds to the total depth of the crater. A reference ToF-SIMS measurement stopped at the diffusion front of the profile indicates that the sputter rate in the diffusion zone does not differ from the sputter rate in the bulk of the sample. We therefore can assume the sputter rate to be constant throughout the ToF-SIMS measurement and linearly transform sputter time into depth. The process for obtaining the crater depth is described in the following.

30

The depth-profiling process formed a crater with a lateral dimension of 300 x 300 μm and a specific depth d_{crater}. The depth of the crater is determined by scanning the topography of the crater

in *x*-axis with a profilometer. An example of the scanned topography is shown in Fig. S2. The crater depth is calculated through the difference in the level in *z*-axis of the sample surface (red colored region) and the valley (blue colored region). The red and blue colored regions also depict the regions in which the step heights are averaged. The process is repeated at two other positions of the crater in order to obtain an averaged value for the crater depth. This value is then used to calculate the sputter rate and convert sputter time into sputter depth.
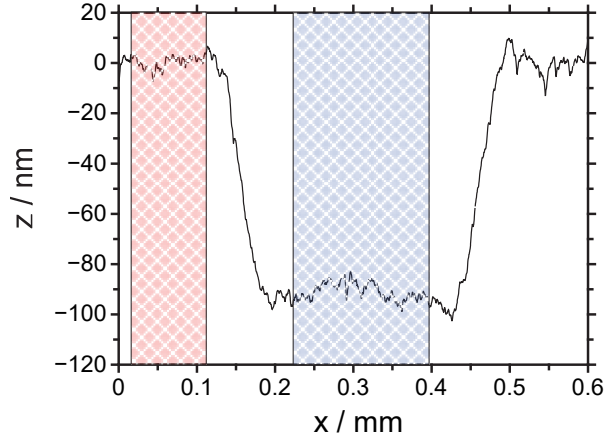
Fig. S2.

Scanned topography through x-axis of a crater. *The scanned topography delivers the crater depth which was measured between the level in z-axis of the sample surface (red colored region) and the valley (blue colored region). The colored regions also depict the regions in which the step heights were averaged. A crater depth of 96.2 nm was obtained from this scanned topography.*

We assume a linear relation between the Poisson corrected ion intensities of the ToF-SIMS measurements,

$$n_{\mathrm{Li}} = a \cdot I_{\mathrm{Li}} \tag{S 1}$$

$$n_{\mathrm{M}} = b \cdot I_{\mathrm{M}} \tag{S 2}$$

where n_{Li} and n_{M} are the native Li ion density and the density of the foreign ion M, I_{Li} and I_{M} are the counts of the ToF-SIMS measurements, and a and b are proportionality constants. Deep in the material, the sample is unchanged and the profile represents the situation in the bulk of the sample. In this regime, the number of Poisson-corrected counts gives the bulk Li ion density (foreign ions from the beam are not present in this regime). We can therefore determine a from the average number of Li counts in the bulk region

$$\frac{n_{\mathrm{Li,bulk}}}{I_{\mathrm{Li,bulk}}^{av}} = a \tag{S 3}$$

The diffusion zone where the foreign ions from the beam have replaced a part of the Li ions is electroneutral in very good approximation. Therefore the foreign ions from the beam replace the native ions in a 1:1 ratio. We can therefore write

$$n_{\mathrm{Li,bulk}} = n_{\mathrm{Li}}(x) + n_{\mathrm{M}}(x) = a \cdot I_{\mathrm{Li}}(x) + b \cdot I_{\mathrm{M}}(x)$$

(S 4)

The proportionality factor b is determined by performing a least- squared error analysis in the replacement zone with respect to the charge conservation condition

$$b = \frac{\sum 2 \cdot n_{\mathrm{Li,bulk}} \cdot I_M(x) - \sum 2 \cdot a \cdot I_{\mathrm{Li}}(x) I_M(x)}{\sum 2 \cdot I_M^2(x)} \, .$$

(S 5)

The sums in this expression run over x-values of the respective diffusion zones. The result of this normalization procedure is shown in Fig. S3.
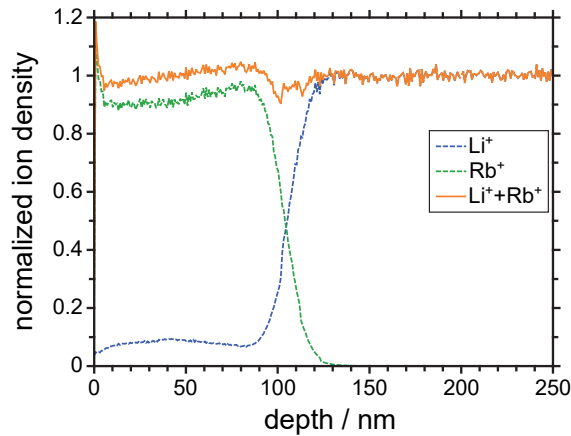
Fig. S3.

Result of the first normalization procedure. *The graphic shows the concentration profiles of Li^+ and Rb^+ as a function of depth below the front surface. Evidently, a zone of 100 nm depth evolved where Rb^+ replaced most of the Li^+. The diffusion front is sharp with a width of about 25 nm. A plateau of Li^+ is observed at 7% of the original bulk Li^+ density in the replacement zone. This plateau corresponds to Li^+ ions immobile during the CAIT experiment. Simulations based on the Nernst-Planck Poisson equations yield a time-independent value of the plateau in good approximation. The orange trace shows the sum of the normalized Li and Rb signals. At the diffusion front and directly at the sample surface, deviations from the bulk ion signal are visible which appear to be caused by small amount of excess charges. The deviation from bulk density is overestimated by the ToF-SIMS measurement.*

At the diffusion front, the normalization does not perfectly work out. Here, the sum of the two normalized signals yields a charge carrier density that is a smaller than the bulk density. The reason for this deviation is that a small amount of charge is accumulated in the diffusion front. Physically, this excess charge must be present because of the modified specific conductivity in the replacement zone, which requires the electric field in the replacement zone to be different from that in the bulk region. Calculations based on the Nernst-Planck-Poisson theory suggest that the charge excess

corresponds to a lack of ion density on the order of less than one ppm of the bulk ion density. However, the ToF-SIMs method overestimates the density lack as charged surfaces reduce the detection probability of the ToF-SIMS machine. As a consequence, a normalization step is introduced where the traces of the charge carriers are scaled such that in sum bulk density is observed (normalization method 1),

$$n_{\text{Li,norm1}}(x) = \frac{n_{\text{Li}}(x)}{n_{\text{Li}}(x)+n_{\text{M}}(x)} ,$$

(S 6)

$$n_{\text{M,norm1}}(x) = \frac{n_{\text{M}}(x)}{n_{\text{Li}}(x)+n_{\text{M}}(x)} .$$

(S 7)

Alternatively, the deviation of the bulk density $\Delta n = n_{\text{Li}}(x) + n_{\text{M}}(x) - n_{\text{Li,bulk}}$ can be evenly distributed to both charge carrier traces (normalization method 2),

$$n_{\text{Li,norm2}}(x) = n_{\text{Li}}(x) - \frac{\Delta n}{2} ,$$

(S 8)

$$n_{\text{M,norm2}}(x) = n_{\text{M}}(x) - \frac{\Delta n}{2}.$$

(S 9)

The two normalization methods represent two extremal cases. Method 1 implies that the error size is proportional to the signal size, and method 2 implies that the error is an absolute error. The true charge carrier density is most likely in between these two extremal cases. The results of the two normalization procedures are shown in Fig. S4.
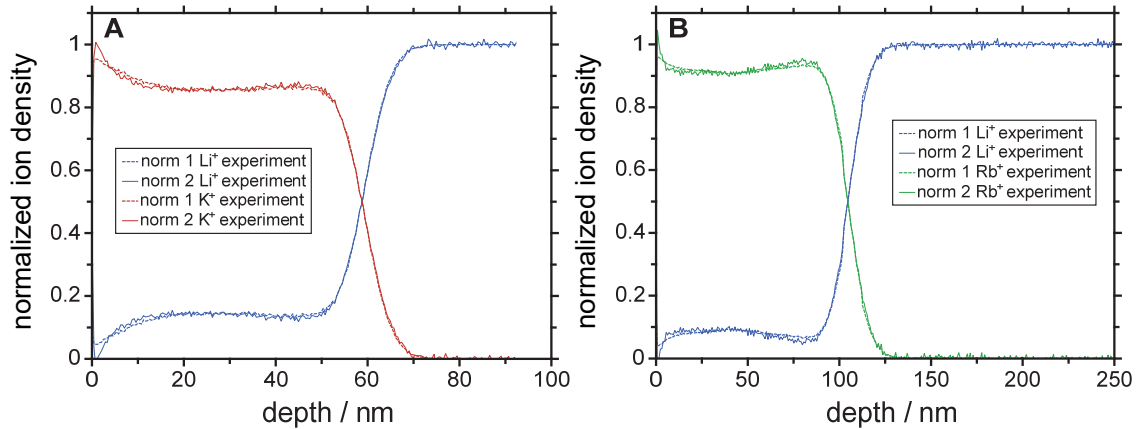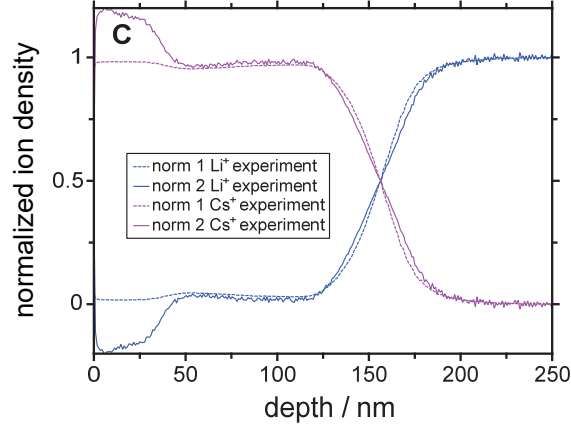
Fig. S4.

Concentration depth profiles of Lithium and the corresponding foreign ion *for the three different CAIT experiments with foreign ions K+ (A), Rb+ (B) and Cs+ (C). The blue lines show the experimental concentration depth profiles of the native Li+ ions. The concentration profiles of K+, Rb+ and Cs+ are shown in red, green and magenta. Each of the profiles shows a plateau of the Li+ concentration in the replacement zone. The plateau is higher for smaller foreign ions. The dashed and solid curves in Fig. S4 A-C refer to the two different normalization methods 1 and 2 discussed above.*

2.4 Nernst-Planck-Poisson equations

The experimental concentration depth profiles are a result of hopping processes within an energetically disordered potential energy landscape. The ion motion starts locally but extends spatially to a long-range regime.

The long-range transport of ions can be modeled within the mathematical framework of coupled Nernst-Planck and Poisson equations that describe the charge carrier transport with effective diffusion coefficients[1,2,3,4].

The ion beam in the CAIT experiment shines homogeneously on a disk like area on the sample surface such hat within this area lateral or angular concentration gradients are not expected. Electric field gradients exist only perpendicular to the sample surface and the aspect ratio of the sample is typically smaller than 1:10. Therefore, we may neglect charge carrier motion in lateral or angular direction and restrict to transport perpendicular to the sample surface. The one-dimensional charge carrier flux density, J_i, is given by the Nernst-Planck equation (for references, see the main text)

$$J_i = -D_i \left(\frac{\partial n_i}{\partial x} + n_i \frac{\partial \varphi}{\partial x} \frac{Z_i e}{k_B T} \right),$$

(S 10)

which describes the transport of the charge carrier species i as a function of a concentration gradient $\partial n_i / \partial x$, an electric potential gradient $\partial \varphi / \partial x$ and the effective diffusion coefficients D_i. The charge of species i is $Z_i e$, and $k_B T$ is Boltzmann's constant times the temperature.

Whenever charge carriers move inside a solid sample, the electric potential inside the sample is affected. In order to account for that effect, the charge carrier distribution and the electric potential have to be treated self-consistently by solving Poisson's equation,

$$\varepsilon_0 \varepsilon_r \frac{\partial^2 \varphi}{\partial x^2} = \sum_i (n_i - n_{i,\text{bulk}}) Z_i e \,. \tag{S 11}$$

Here, ε_r is the dielectric constant (relative permittivity) and ε_0 is the vacuum permittivity. Prior to the CAIT experiment, the charge carrier density equals the bulk density $n_{i,\text{bulk}}$ everywhere in the sample and the glass is electro-neutral. Excess charges arising from the attachment of foreign ions lead to a build-up of a positive surface potential. As the diffusion coefficient of the foreign ion generally differs from the diffusion coefficient of the native ion, the replacement zone exhibits a modified specific conductivity compared to the bulk of the sample. As a consequence, the electric field in the replacement zone is different from the field in the bulk. As a result, a small negative charge accumulation is expected to be present at the diffusion front. Both effects, the charging and the modification of the field are taken into account by Eq. (S11).

Finally, the time dependence of the transport is introduced by Fick's second law that ensures particle number conservation,
$$\frac{\partial n_i}{\partial t} = -\frac{\partial J_i}{\partial x}. \tag{S 12}$$

The boundary conditions of the electric field are defined by the experimental setup and the geometry of the sample. The back-side electrode is grounded such that we set the value of the electric field zero there neglecting offset voltages that could arise due to electrochemical processes. At the front side of the sample a maximum of the electric potential is expected since a grounded aperture is positioned in front of the sample surface. We therefore assume $\frac{\partial \varphi}{\partial x} = 0$ at the front surface of the sample.

Technically, we discretize the sample into space grid elements. The space grid elements are small close to the front surface of the sample where the concentrations change during the experiment and large at the sample back side where the bulk composition remains [1]. The discretization of Poisson's equation (S11) implies that the electric potential in a certain space grid element can be calculated knowing the electric potential in the adjacent space grid elements and the excess charge Q_{ex} in the space grid element of interest [1]. Modification of the electric potential in a certain space element due to charge carrier motion therefore also influences the potential in adjacent increments – an iterative solution of the electric potential is needed.

Initially, the sample is electro-neutral and charge carriers are introduced via the ion beam. Every calculated time step, the potential is updated. The boundary conditions of the electric potential in this case enter the iterative calculation via the first and the last space element. If the space grid contains N elements with their centers x_i and their respective sizes dx_i, the potential iteration at the boundaries of the sample reads

$$\varphi(x_1) = \frac{\varepsilon_0 \varepsilon_r \left(\varphi(x_2) \frac{dx_1}{2} + \left(\varphi(x_1) - \varphi(x_1) \frac{dx_1}{2 d_L} \right) \frac{dx_1 + dx_2}{2} \right) + Q_{ex}(x_1) \frac{dx_1^2}{2} \frac{dx_1 + dx_2}{2}}{\varepsilon_0 \varepsilon_r \frac{dx_1}{2} \frac{dx_1 + dx_2}{2}} \tag{S 13}$$

$$\varphi(x_N) = \frac{\varepsilon_0\varepsilon_r\left(\varphi(x_{N-1})\frac{dx_N}{2}\right) + Q_{ex}(x_1)\frac{dx_N^2}{2}\frac{dx_{N-1} + dx_N}{2}}{\varepsilon_0\varepsilon_r\frac{dx_{N-1} + dx_N}{2}\frac{dx_N}{2}} \qquad \textbf{(S 14)}$$

The condition (S 13) reflects that the electric potential is maximal at the front surface position x_1 and drops in front of the sample surface toward a ground lens that is positioned in a distance d_L. In a physical sense, dx_1 represents the surface roughness of the sample. Potential steps that may stem from the material interface are neglected. The condition (S 13) takes into account that the backside of the sample at position $x_N + dx_N/2$ is grounded. Contact potentials between the glass and the electrode are neglected. Note, that in general $dx_1 \ll dx_N$.

Initially, the sample is filled with bulk concentration of the native ion species. The concentration of the foreign ions from the beam is zero. The ion beam current I_{beam} shining onto the sample surface A introduces a foreign charge carrier flux $J_{beam}=I_{beam}/(ZA)$ into the first space grid element. Z is the charge of the ion species that impinges on the surface. The source current is switched on as long as the potential in the first space grid element does not exceed the repeller potential U_R that defines the kinetic energy of the impinging ions. Else the ion beam is switched off. Ions that reach the back side of the sample are removed from the calculation and their ion current is interpreted as neutralization current.

Knowing the composition and the geometry of the sample, the only free parameters in solving the NPP equations (Eqs. S 10, S11 and S12) are the diffusion coefficients, D_i, of the native and the foreign (external) ion. By matching concentration profiles from experiment and simulation, we have determined the diffusion coefficients.

2.5 Site-energy distribution related macroscopic transport coefficients

We here present a description of the Li diffusion coefficient based on the assumption that the activation energy of the lithium ions is given by the difference between a concentration-independent critical energy and a concentration-dependent Fermi energy of the native lithium ions. The critical energy corresponds to the minimal site energy that needs be surmounted by a single ion for moving over long distances, i.e. to generate long-range transport of the lithium ions.

In the amorphous structure of the glass, the mobile ions move in a disordered potential energy landscape. Directed motion occurs in the presence of a gradient of the electrochemical potential [5,6]. The mobile ions dwell in local energy minima (sites) in the energy landscape and need to overcome energy barriers if they hop from site to site. The distribution of local barriers heights is important for the description of AC experiments where the high frequency of polarity changes restricts the ion motion to the local vicinity of the original site. In CAIT experiments, where a constant voltage is applied for hundreds of hours, a directed motion over a long spatial distance (several hundred nanometer) occurs. In this situation, an effective energy threshold applies that needs to be overcome by the transported ions. The activation barrier of a single ion in this situation, is then defined by the difference between the threshold for long range transport and the original site energy. In the macroscopic analysis of the transport data, the discussion is based on observables, here, the bulk activation energy measured in a reference experiment. The measured activation energies apply to the bulk situation where energetically the site energy distribution (SED) is filled up from the bottom to the topmost occupied energy value – the bulk Fermi energy.

The ions close to the Fermi energy will dominate the measurable ion current and define the detected activation energy.

If a temporally constant external electric field is applied, those ions with the lowest activation energies will move first out of their sites. Restricting the discussion to one single ion species, the occupation of the sites will be depopulated from the top of the site energy distribution to the bottom. As a consequence, the energy difference between the highest occupied sites and the effective threshold energy for the long-range transport rises. Hence, the activation energy rises when the concentration of the ion species decreases. The consequence is a concentration-dependent diffusion coefficient for the ion that is native to the investigated glass.

In order to calculate the relation between the SED and the concentration dependent diffusion coefficient, we consider the SED $S(E)$ resembles a Gaussian function, which can be approximated by a sin²-function. For our CAIT experiments on $Li_3B_7O_{12}$, we assume a bimodal distribution with an energetically higher and lower SED branch, where the lower branch takes into account the presence of immobile Li ions:

$$S(E) = S_1 \frac{2}{\Gamma_1 \pi} \sin^2 \left(\frac{(E-E_0)}{\Gamma_1} + \frac{\pi}{2} \right) + S_2 \frac{2}{\Gamma_2 \pi} \sin^2 \left(\frac{(E-E_0)}{\Gamma_2} + \frac{\pi}{2} + \frac{\pi \Gamma_1}{\Gamma_2} \right).$$ (S 15)

Here, S_i and Γ_i, $i=1,2$, are the total density of available sites and widths of the energetically higher and lower SED branch, respectively, and E_0 is the energetic center of the distribution. S_1 and S_2 define at which concentration the drop of the Li^+-diffusion coefficient is observed. The sum of the two is chosen to be 10% larger than the density of Li^+ ions in the native glass resembling 10% vacant sites. The distribution is filled up from bottom to the top of the SED. The highest occupied energy at bulk density defines the Fermi-energy $E_F(n_{bulk})$ of the Li ions in the native glass. We set the threshold energy for long range transport arbitrarily to zero. Consqently, $E_{act}(n_{bulk}) = 0 - E_F(n_{bulk})$ applies. We therefore set E_0 such that $E_F(n_{bulk}) = -E_{act}(n_{bulk})$ is fulfilled. Since the SED is depopulated from top to bottom, the Fermi level decreases and thus the effective activation energy increases. The concentration dependent activation energy is given by the implicit equation

$$n = \int_{-\infty}^{-E_{act}(n)} S(E) dE.$$ (S 16)

From the activation energy, we can derive the concentration dependent diffusion coefficient via a simple Arrhenius law

$$D(n) = D_0 \exp \left(-\frac{E_{act}(n)}{k_B T} \right),$$ (S 17)

Where D_o is the pre-exponential factor. We determine the conductivity and E_{act} of the unmodified $Li_3B_7O_{12}$ sample in a reference experiment. We then adjust D_o in the NPP calculation to match the experimentally observed conductivity and thereby take into account that concentration and potential gradient contribute to the overall measured sample conductivity.

2.6   Error margin of $D(n)$ and Γ_1

The concentration dependent Li-diffusion coefficient are determined by comparing the result of the NPP calculation versus the experimentally generated profiles. For that purpose a large number of simulations is executed and compared to the experiment. The question arises how sensitive is this analysis with respect to the desired observable $D_{Li}(n)$. In order to realize different $D_{Li}(n)$, Γ_1 in Eq. (S13) is varied corresponding to different widths of the SED of the mobile Li$^+$ ions. A variation of Γ_2 hardly influences the observed profiles as Γ_2 corresponds to the immobile Li$^+$ ions. The influence of different $D_{Li}(n)$ on the concentration profiles is shown in Fig. S5. Sub-figures A and B show the concentration profiles and $D_{Li}(n)$ of the K+-CAIT, subfigures C and D (E and F) show the same for the Rb+-CAIT (Cs+-CAIT). In all the cases Γ_1=0.135 eV (solid), Γ_1=0.16 eV (dashed) and Γ_1=0.18 eV (dotted line) are presented.
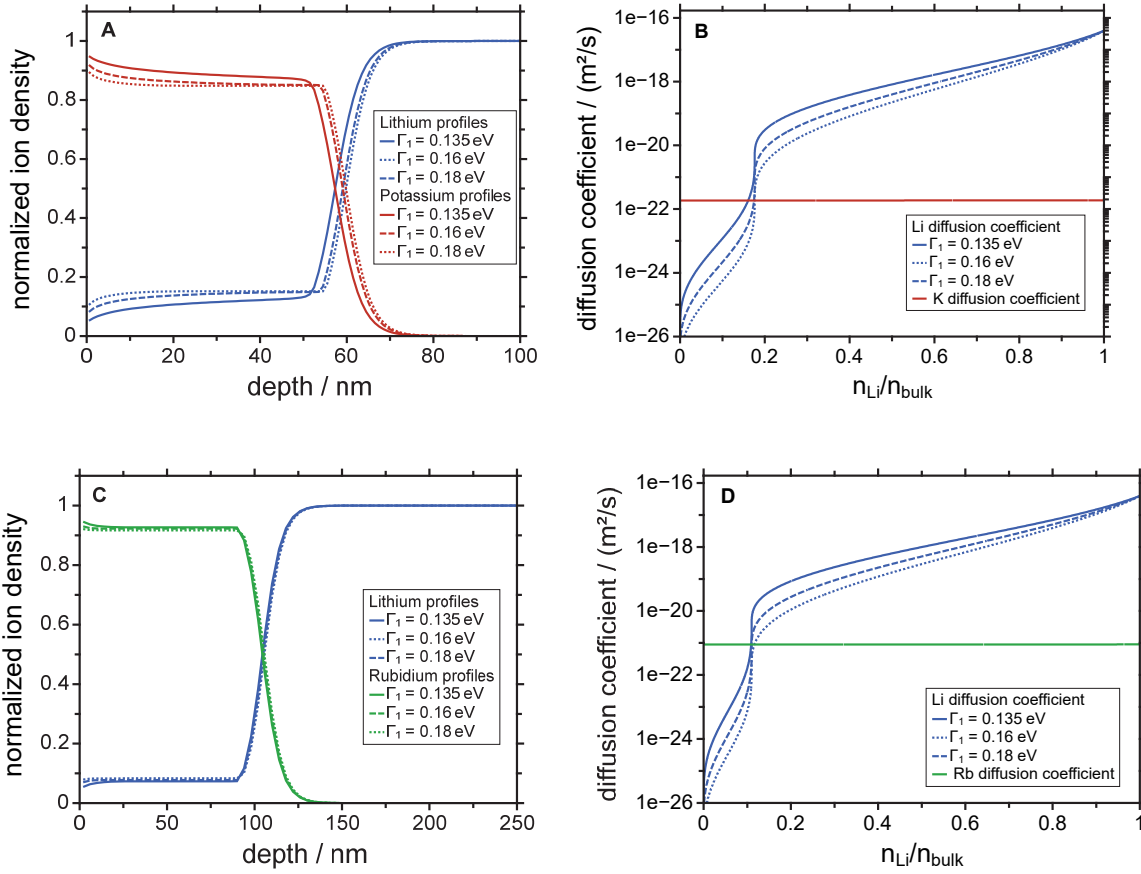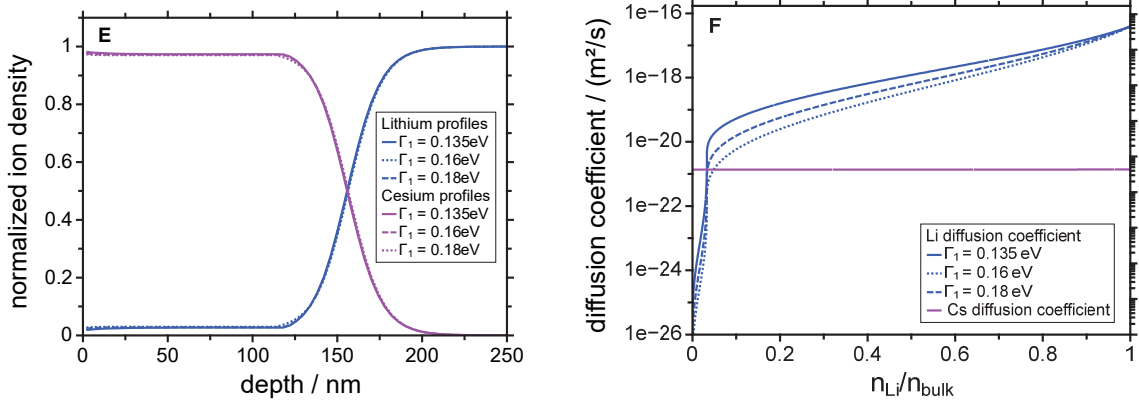
Fig. S5.

Uncertainty of D_Li(n). *The NPP simulations yield concentration profiles that agree with the experimentally measured ones. The error margin within which $D_{Li}(n)$ can be determined is illustrated. Subfigure A shows the concentration profiles of the K-CAIT that are found if the diffusion cofficients given in subfigure B are used in the NPP calculations. Correspondingly, subfigures B and C (D and E) show an analogous variation of $D_{Li}(n)$ for the Rb-CAIT (Cs-CAIT). The variation of $D_{Li}(n)$ is realized by changing the width of the SED of the mobile Li^+ ions Γ_1 (Eq. S12)*

The three Γ_1 values lead to changes in $D_{Li}(n)$ mainly for Li concentrations between $n_{Li}/n_{bulk} = 0.2$ and $n_{Li}/n_{bulk}=0.7$ where $D_{Li}(n)$ varies by a factor of more than 10. However, the different Γ_1 do not affect the Li-bulk diffusion coefficient $D_{Li}(n_{bulk})$ and the concentration at which D_{Li} shows a quick drop with falling concentration: $n_{Li}/n_{bulk} = 0.2$ (K-CAIT), $n_{Li}/n_{bulk} = 0.1$ (Rb-CAIT) and $n_{Li}/n_{bulk} = 0.03$ (Cs-CAIT). In the cases of the Rb- and the Cs-CAIT all three $D_{Li}(n)$ yield similar concentration profiles, in the K-CAIT the shown variation of $D_{Li}(n)$ slightly influences the observed profiles. We are therefore relatively insensitive to changes in $D_{Li}(n)$ at intermediate concentrations between $n_{Li}/n_{bulk} = 0.2$ and $n_{Li}/n_{bulk}=0.7$.

However, already a small change of the bulk diffusion coefficient of less than 5% would lead to profile depths that are incompatible with the experimental findings. The same applies to Li diffusion coefficients in the vicinity of the foreign diffusion coefficients. The concentration at which the native diffusion coefficient intercept and rapidly drops below the foreign diffusion coefficient determines the value of the Li-concentration plateau in the profile which is accurately known. We may state that with decreasing Li^+ concentration $D_{Li}(n)$ must drop quickly at least three orders of magnitude below the foreign diffusion coefficient. Otherwise, the Li-concentration plateau exhibits a significant slope that is not found in either of the experiments. From the comparison between experiment and NPP calculations, we therefore estimate that $\Gamma_1=0.16$ +/- 0.03 eV yields concentration dependencies of $D_{Li}(n)$ giving good agreement between calculated and measured concentration profiles in all three CAIT experiments.

The diffusion coefficient of the foreign ion strongly influences the slope of the diffusion front in the CAIT experiments. A variation of about 10% from the values given in this work already leads to disagreement with the experiment.

2.7   Relation between Onsager transport coefficients and effective diffusion coefficients

We start from the standard Onsager equations for electrochemical transport [7,8,9,10,11].

$$j_1 = -L_{11}\frac{\partial \mu_1^{el.chm.}}{\partial z} - L_{12}\frac{\partial \mu_2^{el.chm.}}{\partial z} \qquad \text{(S 18)}$$

$$j_2 = -L_{21}\frac{\partial \mu_1^{el.chm.}}{\partial z} - L_{22}\frac{\partial \mu_2^{el.chm.}}{\partial z} \qquad \text{(S 19)}$$

Employing $\mu_\alpha^{el.chm.} = q_\alpha\phi + \mu_\alpha$ and applying $\frac{\partial \mu_\alpha}{\partial z} = \sum_\alpha \frac{\partial \mu_\alpha}{\partial n_\alpha}\frac{\partial n_\alpha}{\partial z}$, we find the following set of equation

$$j_1 = -(q_1 L_{11} + q_2 L_{12})\frac{\partial \Phi}{\partial z} - \left(L_{11}\frac{\partial \mu_1}{\partial n_1} + L_{12}\frac{\partial \mu_2}{\partial n_1}\right)\frac{\partial n_1}{\partial z} - \left(L_{11}\frac{\partial \mu_1}{\partial n_2} + L_{12}\frac{\partial \mu_2}{\partial n_2}\right)\frac{\partial n_2}{\partial z} \qquad \text{(S 20)}$$

$$j_2 = -(q_1 L_{22} + q_2 L_{21})\frac{\partial \Phi}{\partial z} - \left(L_{22}\frac{\partial \mu_2}{\partial n_2} + L_{21}\frac{\partial \mu_2}{\partial n_1}\right)\frac{\partial n_2}{\partial z} - \left(L_{22}\frac{\partial \mu_2}{\partial n_2} + L_{21}\frac{\partial \mu_2}{\partial n_1}\right)\frac{\partial n_2}{\partial z} \qquad \text{(S 21)}$$

We evaluate the brackets, sort the terms with respect to the L_{ij} and find

$$\begin{aligned} j_1 = &-(q_1 L_{11} + q_2 L_{12})\frac{\partial \Phi}{\partial z} - L_{11}\left(\frac{\partial \mu_1}{\partial n_1}\frac{\partial n_1}{\partial z} + \frac{\partial \mu_1}{\partial n_2}\frac{\partial n_2}{\partial z}\right) \\ &- L_{12}\left(\frac{\partial \mu_2}{\partial n_1}\frac{\partial n_1}{\partial z} + \frac{\partial \mu_2}{\partial n_2}\frac{\partial n_2}{\partial z}\right) \end{aligned} \qquad \text{(S 22)}$$

$$\begin{aligned} j_2 = &-(q_1 L_{21} + q_2 L_{22})\frac{\partial \Phi}{\partial z} - L_{21}\left(\frac{\partial \mu_1}{\partial n_1}\frac{\partial n_1}{\partial z} + \frac{\partial \mu_1}{\partial n_2}\frac{\partial n_2}{\partial z}\right) \\ &- L_{22}\left(\frac{\partial \mu_2}{\partial n_1}\frac{\partial n_1}{\partial z} + \frac{\partial \mu_2}{\partial n_2}\frac{\partial n_2}{\partial z}\right) \end{aligned} \qquad \text{(S 23)}$$

The CAIT experiment demands several boundary conditions: If the sample of interest is an ion conducting glass, there is usually a very large amount of mobile charge carriers present. In this situation, Poisson's equation enforces charge neutrality in most parts of the sample. A small violation of this condition is found at the diffusion front where a negative or positive excess charge can be present, originating from the fact that the resistivity in the ion exchanged region in general differs from that of the bulk. The number density of charge carriers corresponding to this charge accumulation amounts to less than 0.1 permille of the bulk ion density in most glasses. As a consequence the number density conservation of charge carriers holds throughout the sample in very good approximation for charge carriers with equal charges $q_1=q_2=q$. We may therefore state

$$\sum_{\alpha=1} n_\alpha = n_1 + n_2 = n_{total} := n_{Bulk} \tag{S 24}$$

This condition demands that a 1:1 substitution of native ions by foreign ions and implies for each finite grid element

$$\frac{\partial}{\partial z} \sum_{\alpha=1} n_\alpha = \frac{\partial n_1}{\partial z} + \frac{\partial n_2}{\partial z} = 0 \tag{S 25}$$

$$\partial n_1 + \partial n_2 = 0 \tag{S 26}$$

For the fluxes,

$$dj_1 = -dj_2 \tag{S 27}$$

$$\sum_{\alpha=1} j_\alpha = j_{total} = const \tag{S 28}$$

must hold, otherwise charge accumulation would occur. Since we pointed out above, that Eqs. (S25) and (S26) is obeyed, it follows, that

$$-\frac{\partial n_1}{\partial z} = +\frac{\partial n_2}{\partial z} \tag{S 29}$$

$$-\frac{\partial \mu_1}{\partial n_1} = +\frac{\partial \mu_1}{\partial n_2} \tag{S 30}$$

This leads to the relation

$$
\begin{aligned}
-\frac{\partial \mu_1}{\partial n_1}\frac{\partial n_1}{\partial z} - \frac{\partial \mu_1}{\partial n_2}\frac{\partial n_2}{\partial z} &= -\frac{\partial \mu_1}{\partial n_1}\frac{\partial n_1}{\partial z} + \frac{\partial \mu_1}{\partial n_2}\frac{\partial n_1}{\partial z} \\
&= \left(-\frac{\partial \mu_1}{\partial n_1} + \frac{\partial \mu_1}{\partial n_2}\right)\frac{\partial n_1}{\partial z} \\
&= \left(-\frac{\partial \mu_1}{\partial n_1} - \frac{\partial \mu_1}{\partial n_1}\right)\frac{\partial n_1}{\partial z} \\
&= -2\frac{\partial \mu_1}{\partial n_1}\frac{\partial n_1}{\partial z}
\end{aligned}
\tag{S 31}
$$

We plug relation (S31) into Eqs. (S22) and (S23) and obtain

$$j_1 = -(L_{11} + L_{12})q\frac{\partial \Phi}{\partial z} - 2L_{11}\frac{\partial \mu_1}{\partial n_1}\frac{\partial n_1}{\partial z} - 2L_{12}\frac{\partial \mu_2}{\partial n_1}\frac{\partial n_1}{\partial z} \tag{S 32}$$

14

$$j_2 = -(L_{21} + L_{22})q\frac{\partial \Phi}{\partial z} - 2L_{21}\frac{\partial \mu_1}{\partial n_2}\frac{\partial n_2}{\partial z} - 2L_{22}\frac{\partial \mu_2}{\partial n_2}\frac{\partial n_2}{\partial z} \qquad \text{(S 33)}$$

We observe that in this general expression, the migration part (first term) depends on the diagonal and off-diagonal Onsager coefficients but not on the chemical potential. The chemical diffusion part (second and third term) depends on the chemical potential of both ions and on the diagonal and off-diagonal Onsager coefficients as well.

2.8 Neglecting Onsager Cross-Terms L_{12} and L_{21}

If we neglect the Onsager Cross terms, we find

$$j_1 = -qL_{11}\frac{\partial \Phi}{\partial z} - 2L_{11}\frac{\partial \mu_1}{\partial n_1}\frac{\partial n_1}{\partial z} \qquad \text{(S 34)}$$

$$j_2 = -qL_{22}\frac{\partial \Phi}{\partial z} - 2L_{22}\frac{\partial \mu_2}{\partial n_2}\frac{\partial n_2}{\partial z} \qquad \text{(S 35)}$$

We note, that the gradients $\frac{\partial \Phi}{\partial z}$ and $\frac{\partial n_\alpha}{\partial z}$ also appear in classical Nernst-Planck formalism. In the following we aim at a comparison of the relevant coefficients, possibly enabling physical interpretation.

In order to derive an expression for $2L_{\alpha\alpha}\frac{\partial \mu_\alpha}{\partial n_\alpha}$, let's take a little detour. Here, we shall consider the ideal chemical diffusion of a tracer in whatever, non-interacting medium. Then the particle density flux is given by

$$j_1 = L_{11}\left[-\frac{\partial \mu_1}{\partial n_1}\frac{\partial n_1}{\partial z}\right] = -D_1{}^*\frac{\partial n_1}{\partial z} \qquad \text{(S 36)}$$

$$j_2 = L_{22}\left[-\frac{\partial \mu_2}{\partial n_2}\frac{\partial n_2}{\partial z}\right] = -D_2{}^*\frac{\partial n_2}{\partial z} \qquad \text{(S 37)}$$

where $D_\alpha{}^*$ is the tracer diffusion coefficient of component α. Now the comparison of Eqs. (S36) and (S37) with the chemical part of Eqs. (S34) and (S35) leads to

$$j_1 = -qL_{11}\frac{\partial \Phi}{\partial z} - 2D_1{}^*\frac{\partial n_1}{\partial z} \qquad \text{(S 38)}$$

$$j_2 = -qL_{22}\frac{\partial \Phi}{\partial z} - 2D_2{}^*\frac{\partial n_2}{\partial z} \qquad \text{(S 39)}$$

Thus, the "diffusion" part of the transport equations apparently contains a term $2D^*$. This will become important below.

In the classical NP formalism the particle density flux is given by

$$j_1 = -D_{1,eff} \left(\frac{n_1}{kT} q \frac{\partial \Phi}{\partial z} + \frac{\partial n_1}{\partial z} \right) \qquad \text{(S 40)}$$

$$j_2 = -D_{2,eff} \left(\frac{n_2}{kT} q \frac{\partial \Phi}{\partial z} + \frac{\partial n_2}{\partial z} \right) \qquad \text{(S 41)}$$

Comparison of coefficients leads to the conclusion that

$$L_{11} = D_{1,eff} \frac{n_1}{kT} \qquad \text{(S 42)}$$

$$L_{22} = D_{2,eff} \frac{n_2}{kT} \qquad \text{(S 43)}$$

and

$$D_{1,eff} = 2D_1^* \qquad \text{(S 44)}$$

$$D_{2,eff} = 2D_2^* \qquad \text{(S 45)}$$

The comparison of coefficients, thus implies, that the Onsager equations transform into the classical NP equations under the assumption that Eqs. (S42)-(S45) hold.

Equations (S42) and (S43) ultimately represent what is usually referred to as the Nernst-Einstein relation assuming that the effective diffusion coefficient in the Nernst-Planck formalism is the conductivity derived diffusion coefficient. We direct the reader's attention to standard discussions on the Nernst-Einstein relation including the limits of its approximation [12,13,14,15,16,17].

Equations (S44) and (S45) evidently relate the diffusion coefficient derived from a tracer diffusion experiment to the effective diffusion coefficient used in NP formalism, $D_{\alpha,eff}$. However, if the latter is identified to the conductivity derived diffusion coefficient, then Eqs. (S44) and (S45) transform into the Haven ratio according to

$$\frac{D_\alpha^*}{D_{\alpha,eff}} = \frac{D_\alpha^*}{D_{\alpha,\sigma}} = \; H = 0.5 \qquad \text{(S 46)}$$

Equations (S40) and (S41) represent the form, the NP are implemented in the Marburg transport software [18]. Empirically, for the native ion this $D_{\alpha,eff}$ function has to match the experimentally measured $D_{\alpha,\sigma}$ for the bulk (comparison e.g. to impedance spectroscopy).

For glass systems with relatively high alkali ion content as discussed in the current manuscript, Haven ratios on the order of 0.5 or below are in fact commonly observed in experiments. [19,20] Thus, the consideration presented above is at the least self-consistent. The question remains, whether it contains more than a proof of self-consistency. This relates to question of the "ideal" Haven ratio to be observed for non-interacting particles in a tracer diffusion experiment reflecting ideal solutions. According to Murch, the ideal Haven ratio should be identical to 1 [21,13], based on the assumption that in an ideal solution tracer experiment the relevant activity coefficient should be 1 and the transport coefficient measured should be identical to the one measured in a conductivity experiment. We will come back to the situation H = 1 at a later point.

In this context it is import to realize that not only the interpretation of diffusion coefficients measured in different experimental concepts is very different[13], the concept of diagonal and non-diagonal Onsager coefficients may also have to be adopted to a specific experimental approach considered. There is no unique diffusion coefficient [22,23,24,25,20,26] and there is perhaps not a unique Onsager coefficient either.

Elaborating the relevant gradients of the chemical potential as presented above suggests that the ideal Haven ratio might rather be 0.5 instead of 1. To further support this point we consider in the following the Onsager equations for transport in a gradient of the chemical potential only (absence of an electric field).

Let's, for this, consider a hypothetical tracer experiment with strong correlation between μ_1 of species 1 diffusing into the target, and μ_2 of species 2 diffusing out of the target (opposite directions !). Hence, we chose to make use of the chemical part of Eq. (S22), in other words, we consider the flux to be given by (neglecting cross Onsager terms)

$$j_1 = L_{11}\left[-\frac{\partial \mu_1}{\partial n_1}\frac{\partial n_1}{\partial z} - \frac{\partial \mu_1}{\partial n_2}\frac{\partial n_2}{\partial z}\right] \tag{S 47}$$

In a tracer experiment the two species move in opposite direction; the flux has a different sign. On a one-dimensional grid with z pointing to the right, we can define, $\Delta z = z_{final} - z_{initial}$. This gives Δz a different sign for the native tracer and the external tracer. Therefore, while Eq. (S26) still holds, we arrive at

$$\frac{\partial n_1}{\partial z} = \frac{\partial n_2}{\partial z} \tag{S 48}$$

This is different from Eq. (S29) and (S30) ! Combining this, leads to

$$-\frac{\partial \mu_1}{\partial n_1}\frac{\partial n_1}{\partial z} - \frac{\partial \mu_1}{\partial n_2}\frac{\partial n_2}{\partial z} = \left(-\frac{\partial \mu_1}{\partial n_1} - \frac{\partial \mu_1}{\partial n_2}\right)\frac{\partial n_1}{\partial z} \tag{S 49}$$

Since $dn_1 = -dn_2$ (Eq. (S39)) holds, we have

$$-\frac{\partial \mu_1}{\partial n_1}\frac{\partial n_1}{\partial z} - \frac{\partial \mu_1}{\partial n_2}\frac{\partial n_2}{\partial z} = \left(-\frac{\partial \mu_1}{\partial n_1} + \frac{\partial \mu_1}{\partial n_1}\right)\frac{\partial n_1}{\partial z} = 0 \tag{S 50}$$

As a consequence, the flux becomes ZERO in the case of bidirectional tracer diffusion with "perfect" correlation between the species. This may sound strange in the first place, but should have been expected.

Let's remember the discussion of Haven ratios, $H = D^* / D_\sigma$, where D^* is a tracer diffusion coefficient and D_σ is the conductivity related diffusion coefficient. Empirically, this ratio is often $H = 0.5$ (or 0.4) in the case of perfectly un-correlated tracers. With increasing amount of correlation, the Haven ratio normally decreases. The consideration above suggests that for "perfect correlation" (this term would eventually need to be defined more precisely) D^* approaches zero and the Haven ratio also approaches zero.

Haven ratio in dilute alkali glasses

Having discussed the cases H=0.5 and H=0 above, we now return to the limiting case H=1. In fact, Haven ratios close to 1 have been reported by Thomas et al. in very dilute Sodium Silicate glasses for molar fractions of less than 1 mol% Na_2O [27]. With increasing molar fraction, the Haven ratio swiftly drops to the typical value around 0.5. Estimates from Lammert et al. show that under these dilute conditions not only the site density but also the density of vacancies is very low [28]. Tomazawa et al. conclude that for very low alkali content in Borate glasses the transport mechanism of the alkali ions is given by an interstitial transport rather than by hopping from site to site [29]. The latter would involve vacancies, which may be hundreds of Angstrom apart for such low dilution.

In such a situation, Alkali ions entering the glass may not necessarily replace native ions. The foreign ions occupy interstitials. Locally the particle density (foreign ion density plus native ion density) is not any more strictly conserved. Foreign and native alkali ions hence may move independently from each other – the chemical potential of one ion species does not depend on the concentration of the other ion species. In that case Eq. (S 30) becomes

$$\frac{\partial \mu_2}{\partial n_1} = \frac{\partial \mu_1}{\partial n_2} = 0 \qquad \textbf{(S 51)}$$

Plugging this into Eqs. (S20 and S21), and setting $q_1 = q_2 = q$, we find

$$j_1 = -(L_{11} + L_{12})q\frac{\partial \Phi}{\partial z} - L_{11}\frac{\partial \mu_1}{\partial n_1}\frac{\partial n_1}{\partial z} - L_{12}\frac{\partial \mu_2}{\partial n_2}\frac{\partial n_2}{\partial z} \qquad \textbf{(S 52)}$$

$$j_2 = -(L_{21} + L_{22})q\frac{\partial \Phi}{\partial z} - L_{21}\frac{\partial \mu_1}{\partial n_1}\frac{\partial n_1}{\partial z} - L_{22}\frac{\partial \mu_2}{\partial n_2}\frac{\partial n_2}{\partial z} \qquad \textbf{(S 53)}$$

Note that compared to Eqs. (S32) and (S33) the factor of 2 in the second term is missing. Neglecting the Onsager cross terms L_{12} and L_{21} yields

$$j_1 = -qL_{11}\frac{\partial \Phi}{\partial z} - L_{11}\frac{\partial \mu_1}{\partial n_1}\frac{\partial n_1}{\partial z} \qquad \textbf{(S 54)}$$

$$j_2 = -qL_{22}\frac{\partial \Phi}{\partial z} - L_{22}\frac{\partial \mu_2}{\partial n_2}\frac{\partial n_2}{\partial z} \qquad \textbf{(S 55)}$$

Comparison to NPP and Nernst-Einstein-Relation we eventually end up with

$$\frac{D_\alpha^*}{D_{\alpha,eff}} = \frac{D_\alpha^*}{D_{\alpha,\sigma}} = H = 1 \qquad \textbf{(S 56)}$$

as suggested by the experimental observations. As a consequence, the situation H=1 arises from a characteristic of the transport mechanism, i.e., interstitial instead of vacancy transport. In total, the treatise presented above provided plausible constellations, where in all cases the Haven ratio is $H \leq 1$, in line with suggestions in the literature. [30]

As a consequence, the cross relation of the chemical potential on both ion species (Eq. (S32)) does not lead to an obstacle. To the contrary, it leads to the conclusion that unidirectional and hence correlated transport of ions in one direction requires a term $2D_\alpha^*$ in the diffusion term, with a classical Haven ratio concept. This concept inherently takes into account that in the CAIT experiment the native ion is forced to move up-hill in the concentration domain. In the CAIT experiment the translocation up the concentration hill of the native ion is enforced by the electric field, hence this constitutes electro-diffusion. There are other well-known examples of "up-hill" diffusion in the concentration domain, which are of course down-hill in the chemical potential domain. The diffusion of carbon in austenitic steels differing in the silicon content is a prominent example [31,32,33]. The situation of uni-directional electrodiffusion is different from bi-directional classical tracer diffusion.

So far, no assumption regarding the form of the chemical potential function has been employed. The only de facto assumption implied is that Eqs. (S44) and (S45) hold, even once the concentration dependence of D or L is explicitly accounted for.

The line of arguments presented above is considered to demonstrate that Eqs. (S44) and (S45) are plausible and the description is self-consistent. With the current information we are not in the position to exclude that the ratio between D* / D_σ, has a value different from 0.5. We expect being able to directly determine D* / D_σ within the CAIT concept e.g. by performing successive CAIT experiments under varied conditions.

2.9   Including Onsager cross terms L_{12}, L_{21}

The transport equations including the Onsager cross terms is given by Eqs. (S32) and (S33)

$$j_1 = -(L_{11} + L_{12})q\frac{\partial \Phi}{\partial z} - 2L_{11}\frac{\partial \mu_1}{\partial n_1}\frac{\partial n_1}{\partial z} - 2L_{12}\frac{\partial \mu_2}{\partial n_1}\frac{\partial n_1}{\partial z} \qquad \text{(S 57)}$$

$$j_2 = -(L_{21} + L_{22})q\frac{\partial \Phi}{\partial z} - 2L_{21}\frac{\partial \mu_1}{\partial n_2}\frac{\partial n_2}{\partial z} - 2L_{22}\frac{\partial \mu_2}{\partial n_2}\frac{\partial n_2}{\partial z} \qquad \text{(S 58)}$$

In the two chemical diffusion terms, dn/dz can be factored out

$$j_1 = -(L_{11} + L_{12})q\frac{\partial \Phi}{\partial z} - 2\left(\frac{L_{11}}{T}\frac{\partial \mu_1}{\partial n_1} + \frac{L_{12}}{T}\frac{\partial \mu_2}{\partial n_1}\right)\frac{\partial n_1}{\partial z} \qquad \text{(S 59)}$$

$$j_2 = -(L_{21} + L_{22})q\frac{\partial \Phi}{\partial z} - 2\left(\frac{L_{21}}{T}\frac{\partial \mu_1}{\partial n_2} + \frac{L_{22}}{T}\frac{\partial \mu_2}{\partial n_2}\right)\frac{\partial n_2}{\partial z} \qquad \text{(S 60)}$$

In analogy to the argument presented above, we can now directly compare the coefficients of the classical NP equations and identify

$$D_{1,\sigma} = \frac{kT}{n_1}(L_{11} + L_{12}) \qquad \text{(S 61)}$$

$$D_{2,\sigma} = \frac{kT}{n_2}(L_{21} + L_{22})$$

<div align="right">(S 62)</div>

and

$$D_1^* = L_{11}\frac{\partial \mu_1}{\partial n_1} + L_{12}\frac{\partial \mu_2}{\partial n_1}$$

<div align="right">(S 63)</div>

$$D_2^* = L_{21}\frac{\partial \mu_1}{\partial n_2} + L_{22}\frac{\partial \mu_2}{\partial n_2}$$

<div align="right">(S 64)</div>

Combining Eqs. (S55)-(S58), as well as $2D_\alpha^* = D_{\alpha,\sigma}$, with Eqs. (S59) and (S60) yields

$$j_1 = -D_{1,\sigma}\left(\frac{qn_1}{kT}\frac{\partial \Phi}{\partial z} + \frac{\partial n_1}{\partial z}\right)$$

<div align="right">(S 65)</div>

$$j_2 = -D_{2,\sigma}\left(\frac{qn_2}{kT}\frac{\partial \Phi}{\partial z} + \frac{\partial n_2}{\partial z}\right)$$

<div align="right">(S 66)</div>

This is again the classical form of a set of Nernst-Planck equations. This format can always be derived, even if $D_{\alpha,\sigma}$, and D_α^* explicitly depend on the density of the other ion type β. The reason is that n_α can always be expressed as $n_{bulk} - n_\beta$, according to Eq. (S24). This is valid independent of the explicit shape of μ_α. We therefore end up with an equation with similar form as Eqs. (S42) and (S43). The difference between Eqs.(S42)-(S45) and Eqs.(S61)-(S64) concerns the interpretation of the transport coefficients $D_{\alpha,\sigma}$ and D_α^* which in the different approximations is given by different combinations of $L_{\alpha\beta}$.

2.10 Constant foreign diffusion coefficient

We find best agreement between experimental profiles and the profiles calculated by means of the Nernst-Planck equations if the foreign diffusion coefficient is assumed to be concentration independent. The profiles observed from the CAIT experiments on the Li$_3$B$_7$O$_{12}$ glass allow us to analytically calculate the constant foreign diffusion coefficient in very good approximation.
We start from a schematic drawing of the profiles that consist of three distinctly different regions: the diffusion zone (D), the diffusion front (F) and the bulk (B).

diffusion zone (D)   bulk (B)

diffusion front (F)
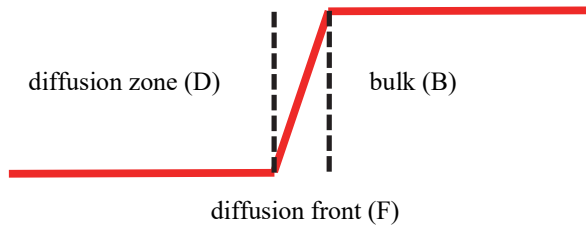
Scheme 1: Illustration of three different zones discussed for the derivation of an analytical relation between $D_{foreign}$ and D_{native}.

In the bulk, only native ions are present (index 1). Concentration gradients are absent here. In the diffusion zone, native ions have been replaced by foreign ions (index 2). In this zone, the concentration variation is only small and a spatially and temporally constant native ion plateau is observed. The concentration changes mainly occur at the diffusion front. In a quasi-stationary situation where the same number of ions reach the front side of the sample as are neutralized at its back side, the total ion flux becomes space (and time) independent.

$$\sum_{i=1,2} J_i = J_{tot} = const \tag{S 67}$$

where J_{tot} is the sum of all ion fluxes. We assume that the Nernst-Planck equation applies in all three parts of the sample

$$J_i = -D_i\left(\nabla n_i + n_i \nabla\varphi \frac{Z_i e}{k_B T}\right) \tag{S 68}$$

In the bulk region of the sample, foreign charge carriers are not present and spatial concentration gradients are absent such that $J_{tot} = J_1$ and $\nabla n_1 = 0$ holds. The total ion flux in bulk is then given by

$$J_{tot} = J_1^B = -D_1^B n_1^B E^B \tag{S 69}$$

where D_1^B is the native bulk diffusion coefficient, n_1^B is the native bulk ion density and $E^B = -\frac{U_R - \Delta U_D}{L - L_D}\frac{e}{k_B T}$ is the electric field in the bulk times e/(k$_B$T), with the repeller voltage U_R, the voltage drop across the diffusion zone ΔU_D, the thickness of the sample L and the thickness of the diffusion zone L_D. In the diffusion zone, the total ion flux is given by

$$J_{tot} = J_1^D + J_2^D = -D_1^D n_1^D E^D - D_2^D (n_1^B - n_1^D) E^D \tag{S 70}$$

where the superscript D indicates the respective quantities in the diffusion zone, $n_1^B - n_1^D = n_2^D$ is the density of the foreign species in the diffusion zone and $E^D = -\frac{\Delta U_D}{L_D}\frac{e}{k_B T}$ is the electric field in the diffusion zone times $\frac{e}{k_B T}$. Since the total ion flux is space independent, $J_1^B = J_1^D + J_2^D$ holds.

$$D_1^B n_1^B E^B = D_1^D n_1^D E^D + D_2^D (n_1^B - n_1^D) E^D$$

$$= [D_1^D n_1^D + D_2^D (n_1^B - n_1^D)] E^D \tag{S 71}$$

Dividing by the term in the brackets yields an expression for E^D

$$E^D = \frac{D_1^B n_1^B E^B}{D_1^D n_1^D + D_2^D (n_1^B - n_1^D)} \tag{S 72}$$

The total ion flux in the diffusion zone is given by

$$\begin{aligned} J_{tot} = J_1^F + J_2^F &= -D_1^F (\nabla n_1 + n_1^F E^F) - D_2^F (\nabla n_2 + n_2^F E^F) \\ &= -D_1^F (\nabla n_1 + n_1^F E^F) - D_2^F (-\nabla n_1 + (n_1^B - n_1^F) E^F) \end{aligned} \tag{S 73}$$

where $\nabla n_2 = -\nabla n_1$ and $n_2^F = (n_1^B - n_1^F)$ have been used. Applying the space independence of the flux density yields:

$$D_1^B n_1^B E^B = D_1^F (\nabla n_1 + n_1^F E^F) + D_2^F (-\nabla n_1 + (n_1^B - n_1^F) E^F) \tag{S 74}$$

This condition must essentially hold at any position of the diffusion front. We choose a point at the center of the diffusion front and assume

$$n_1^F = \frac{n_1^B + n_1^D}{2} \tag{S 75}$$

$$E^F = \frac{E^B + E^D}{2} \tag{S 76}$$

For the Li₃B₇O₁₂ profiles shown in the main manuscript, the diffusion coefficient of the native ion was far larger than the diffusion coefficient of the foreign ion at about 55% bulk concentration corresponding to $n_1^F = \frac{n_1^B + n_1^D}{2}$. Under these conditions,

$$D_1^F (\nabla n_1 + n_1^F E^F) > D_2^F (-\nabla n_1 + (n_1^B - n_1^F) E^F) \tag{S 77}$$

is valid which leads to

$$\begin{aligned} D_1^B n_1^B E^B &= D_1^F \left(\nabla n_1 + \frac{n_1^B + n_1^D}{2} \frac{E^B + E^D}{2} \right) \\ &= D_1^F \nabla n_1 + \frac{D_1^F}{4} (n_1^B + n_1^D)(E^B + E^D) \end{aligned} \tag{S 78}$$

Plugging in Eq. (S72), resolving with respect to D_2^D leads to the result

$$D_2^D = D_1^B \frac{(n_1^B + n_1^D)}{(n_1^B - n_1^D)} \cdot \frac{n_1^B}{4\frac{D_1^B}{D_1^F}n_1^B - \frac{4}{E^B}\nabla n_1 - (n_1^B + n_1^D)} - D_1^D \frac{n_1^D}{(n_1^B - n_1^D)} \qquad \textbf{(S 79)}$$

We may evaluate Eq. (S79) by plugging in the electric field in the bulk as well as the concentrations observed in the concentration profiles. The diffusion coefficient of the Li ions is taken from the best match between experiment and NPP calculation.

	K-CAIT	Rb-CAIT	Cs-CAIT
$n_{Li}^D/(m^{-3})$	$1.96 \cdot 10^{27}$	$1.12 \cdot 10^{27}$	$4.2 \cdot 10^{26}$
$n_{Li}^B/(m^{-3})$	$1.40 \cdot 10^{28}$	$1.40 \cdot 10^{28}$	$1.40 \cdot 10^{28}$
$D_{Li}^B/(m^2/s)$	$3.9 \cdot 10^{-17}$	$3.9 \cdot 10^{-17}$	$3.9 \cdot 10^{-17}$
$D_{Li}^F/(m^2/s)$	$3.72 \cdot 10^{-19}$	$7.08 \cdot 10^{-19}$	$7.08 \cdot 10^{-19}$
$D_{Li}^D/(m^2/s)$	$1.1 \cdot 10^{-22}$	$1.00 \cdot 10^{-23}$	$2.62 \cdot 10^{-23}$
$E^B/(1/m)$	$-1.427 \cdot 10^3$	$-3.97 \cdot 10^3$	$-3.40 \cdot 10^3$
$\nabla n_{Li}^F/(1/m^4)$	$1.19 \cdot 10^{36}$	$3.30 \cdot 10^{35}$	$3.43 \cdot 10^{35}$

Table 1: parameters used to calculate D_2^D

Evaluating Eq. (S30) with the parameters from table 1, we find

Experiment	D_2^D from Eq. (38) / (m²/s)	D_2 best match / (m²/s)
K-CAIT	$2.01 \cdot 10^{-22}$	$1.87 \cdot 10^{-22}$
Rb-CAIT	$1.00 \cdot 10^{-21}$	$0.90 \cdot 10^{-21}$
Cs-CAIT	$1.43 \cdot 10^{-21}$	$1.36 \cdot 10^{-21}$

Table 2: comparison between foreign diffusion coefficients derived from Eq. (S30) and the foreign diffusion coefficient from the full NPP calculations leading to best match between experiment and theory.

We conclude that for a situation, where the bulk diffusion coefficient of the native ion is significantly larger than the diffusion coefficient of the foreign ion in the diffusion front, the latter is effectively fixed to a single value determined solely by properties of the native ion and the electric field operative in the bulk. Consequently, in a situation where the foreign ion diffusion coefficient is larger than that of the native ion, the characteristics are reversed. In that case, the diffusion coefficient of the foreign ion appears as concentration dependent and the diffusion coefficient of the native ion appears concentration independent. This is in fact supported by an experiment, where a K$^+$ ion beam was shined at a Rb$^+$ ion conductor [34].

References

1. M. Schäfer and K.-M. Weitzel: 'Bombardment induced ion transport. Part I: Numerical investigation of bombardment induced ion transport through glasses and membranes on the basis of the Nernst-Planck-Poisson equations', *Physical Chemistry Chemical Physics : PCCP*, 2011, **13**(45), 20112–20122, doi: 10.1039/c1cp21215j.

2. P. V. Menezes, J. Martin, M. Schäfer, H. Staesche, B. Roling, and K.-M. Weitzel: 'Bombardment induced ion transport--part II. Experimental potassium ion conductivities in borosilicate glass', *Physical Chemistry Chemical Physics : PCCP*, 2011, **13**(45), 20123–20128, doi: 10.1039/c1cp21216h.

3. M. Schäfer, D. Budina, and K.-M. Weitzel: 'Site energy distribution of sodium ions in a sodium rubidium borate glass', *Physical Chemistry Chemical Physics : PCCP*, 2019, **21**(47), 26251–26261, doi: 10.1039/c9cp05194e.

4. M. Schäfer and K.-M. Weitzel: 'Site energy distribution of ions in the potential energy landscape of amorphous solids', *Materials Today Physics*, 2018, **5**(3), 12–19, doi: 10.1016/j.mtphys.2018.05.002.

5. R. Kirchheim: 'The mixed alkali effect as a consequence of network density and site energy distribution', *J. Non-Cryst. Solids*, 2000, **272**(2-3), 85–102.

6. R. Kirchheim and D. Paulmann: 'The relevance of site energy distribution for the mixed alkali effect', *J. Non-Cryst. Solids*, 2001, **286**(3), 210–223.

7. L. Onsager: 'Reciprocal relations in irreversible processes. I', *Phys. Rev.*, 1931, **37**(4), 405–426, doi: 10.1103/PhysRev.37.405.

8. C. Chatzichristodoulou, W.-S. Park, H.-S. Kim, P. V. Hendriksen, and H.-I. Yoo: 'Experimental determination of the Onsager coefficients of transport for Ce(0.8)Pr(0.2)O(2-delta)', *Physical Chemistry Chemical Physics : PCCP*, 2010, **12**(33), 9637–9649, doi: 10.1039/c000865f.

9. M. Martin: 'Diffusion in Oxides', in 'Diffusion in condensed matter: Methods, materials, models', (ed. P. Heitjans and J. Kärger), p. 226; 2005, Berlin, Heidelberg, Springer.

10. M. Landstorfer and T. Jacob: 'Mathematical modeling of intercalation batteries at the cell level and beyond', *Chemical Society reviews*, 2013, **42**(8), 3234–3252, doi: 10.1039/c2cs35050e.

11. K. D. Fong, H. K. Bergstrom, B. D. McCloskey, and K. K. Mandadapu: 'Transport phenomena in electrolyte solutions: Nonequilibrium thermodynamics and statistical mechanics', *AIChE Journal*, 2020, **66**(12), doi: 10.1002/aic.17091.

12. C. M. A. Brett and A. M. Oliveira Brett: 'Electrochemistry: Principles, methods, and applications', 1st edn; 2005, Oxford, Oxford Univ. Press.

13. G. E. Murch: 'Diffusion Kinetics in Solids', in 'Phase transformations in materials', (ed. G. Kostorz and G. Kostorz), 171–238; 2001, Weinheim, New York, Chichester, Wiley-VCH.

14. R. A. McKee: 'A generalization of the nernst-Einstein equation for self-diffusion in high defect concentration solids', *Solid State Ionics*, 1981, **5**, 133–136, doi: 10.1016/0167-2738(81)90210-1.

15. G. Peskir: 'On the Diffusion Coefficient: The Einstein Relation and Beyond', *Stochastic Models*, 2003, **19**(3), 383–405, doi: 10.1081/STM-120023566.

16. M.-C. Pang, M. Marinescu, H. Wang, and G. Offer: 'Mechanical behaviour of inorganic solid-state batteries: can we model the ionic mobility in the electrolyte with Nernst-

Einstein's relation?', *Physical Chemistry Chemical Physics : PCCP*, 2021, **23**(48), 27159–27170, doi: 10.1039/D1CP00909E.

17. Z. Li, R. P. Misra, Y. Li, Y.-C. Yao, S. Zhao, Y. Zhang, Y. Chen, D. Blankschtein, and A. Noy: 'Breakdown of the Nernst-Einstein relation in carbon nanotube porins', *Nat. Nanotechnol.*, 2023, **18**(2), 177–183, doi: 10.1038/s41565-022-01276-0.

18. M. Schäfer and K.-M. Weitzel: 'The Marburg program suit for modelling charge carrier transport in solids', *to be published*.

19. J. O. Isard: 'The Haven ratio in glasses', *J. Non-Cryst. Solids*, 1999, **246**(1), 16–26, doi: 10.1016/S0022-3093(99)00036-8.

20. H. Mehrer: 'Diffusion in Solids -- Fundamentals, Methods, Materials, Diffusion-Controlled Processes'; 2007, Berlin, Heidelberg, Springer-Verlag.

21. G. MURCH: 'The haven ratio in fast ionic conductors', *Solid State Ionics*, 1982, **7**(3), 177–198, doi: 10.1016/0167-2738(82)90050-9.

22. J. Maier: 'Physical chemistry of ionic materials: Ions and electrons in solids'; 2023, Hoboken, NJ, Wiley.

23. C. Wagner: 'Equations for transport in solid oxides and sulfides of transition metals', *Progress in Solid State Chemistry*, 1975, **10**, 3–16, doi: 10.1016/0079-6786(75)90002-3.

24. H. Schmalzried: 'Chemical Kinetics of Solids', 1st edn; 2008, Weinheim, Wiley-VCH.

25. P. Heitjans and J. Kärger (eds.): 'Diffusion in condensed matter: Methods, materials, models'; 2005, Berlin, Heidelberg, Springer.

26. S. Chakraborty and J. Ganguly: 'Cation diffusion in aluminosilicate garnets: experimental determination in spessartine-almandine diffusion couples, evaluation of effective binary diffusion coefficients, and applications', *Contrib Mineral Petrol*, 1992, **111**(1), 74–86, doi: 10.1007/BF00296579.

27. M. Thomas and N. Peterson: 'Electrical conductivity and tracer diffusion in sodium germanate glasses☆', *Solid State Ionics*, 1984, **14**(4), 297–307, doi: 10.1016/0167-2738(84)90114-0.

28. H. Lammert, M. Kunow, and A. Heuer: 'Complete Identification of Alkali Sites in Ion Conducting Lithium Silicate Glasses: A Computer Study of Ion Dynamics', *Phys. Rev. Lett.*, 2003, **90**, 215901, doi: 10.1103/PhysRevLett.90.215901.

29. M. Tomozawa: 'The mixed alkali effect and thermodynamic state of glasses', *Solid State Ionics*, 1998, **105**(1-4), 249–255, doi: 10.1016/S0167-2738(97)00472-4.

30. H. K. Kashyap, H. V. R. Annapureddy, F. O. Raineri, and C. J. Margulis: 'How is charge transport different in ionic liquids and electrolyte solutions?', *The journal of physical chemistry. B*, 2011, **115**(45), 13212–13221, doi: 10.1021/jp204182c.

31. Darken L. S.: 'Diffusion of carbon in austenite with a discontinuity in composition', *Trans. AIME.*, 1949, **180**, 430–438.

32. M. Colangeli, A. de Masi, and E. Presutti: 'Microscopic models for uphill diffusion', *J. Phys. A: Math. Theor.*, 2017, **50**(43), 435002, doi: 10.1088/1751-8121/aa8c68.

33. R. Krishna: 'Uphill diffusion in multicomponent mixtures', *Chemical Society reviews*, 2015, **44**(10), 2812–2836, doi: 10.1039/c4cs00440j.

34. D. Budina, J. Zakel, J. Martin, P. Menezes, M. Schaefer, and K.-M. Weitzel: 'Bombardment Induced Transport of Rb+ through a K+ Conducting Glass vs. K+ Transport through a Rb+ Conducting Glass', *Z. Phys. Chem.*, 2014, **228**(4-5, SI), 609–627, doi: 10.1515/zpch-2014-0459.